Int. J. Electrochem. Sci., 12 **(2017)** 7518 – 7536, doi: 10.20964/2017.08.12

International Journal of
ELECTROCHEMICAL
SCIENCE
www.electrochemsci.org

Dynamic Modeling and Fractional Order PI$^{\lambda}$D$^{\mu}$ Control of PEM Fuel Cell

Xueqin Lü[1,*] , *Xing Miao*[1], *Yang Xue*[1], *Liang Deng*[1],*Min Wang*[1], *Dongxia Gu*[1], *Xinyu Li*[1]

School of Automation Engineering, Shanghai University of Electric Power, Shanghai 200090, China
[*]E-mail: lvxueqin@shiep.edu.cn

Received: 30 January 2017 / *Accepted:* 24 May 2017 / *Published:* 12 July 2017

In order to improve the dynamic performance and efficiency of the proton exchange membrane fuel cell (PEMFC), a fractional order PI$^{\lambda}$D$^{\mu}$ (FOPID) controller is proposed. The electrical characteristic of PEMFC are described by the lumped parameter model, which is verified accurately in this paper. The controller uses the hydrogen pressure as the control variable to control the PEMFC output voltage. At the same time, an improved Oustaloup filter algorithm is adopted to approximate the fractional calculus operator (s^r, $r \in$ R) in the controller which is an extension of the Oustaloup method. Moreover, the performance of the PEMFC control system is carried out on a real-time virtual test system, which is based on the Labview simulation interface toolkit and MATLAB/simulink. The validation results show that, compared to the PID control method, the FOPID control method has the advantages of smaller overshoot, faster response, better stability, and the operation efficiency of the PEMFC has increased by 0.6%. In addition, the virtual test system is greatly shorts the test time, reflects the process of testing and has a high degree of visualization.

Keywords: PEMFC, FOPID control, Nonlinear system, Dynamic performance, Labview

1. INTRODUCTION

With the coming of industry 4.0, the modern industrial cable robots need to be gradually upgraded to the cable less robots to adapt to the complex on-site manufacturing environment. At present, the cable power supply limits the motion and the flexibility of the robots [1]. It is necessary to find an effective matching energy as the drive to replace the traditional cable. The proton exchange membrane fuel cell (PEMFC) has the advantages of low operating temperature, fast power response, high power density, low corrosion, and environmental friendliness. It is an important alternative to the traditional cable robot [2-4].

When the PEMFC runs smoothly, it usually involves electrochemistry, hydrodynamics and thermodynamics. Therefore, the PEMFC system owns the characteristics of complex mechanism, dynamic coupling and response lag [5]. It is important to study the dynamic characteristics of PEMFC for understanding its operating mechanism, optimizing the cell structure and controlling the system. Therefore, in recent years, the dynamic characteristics of fuel cell research has become a hot topic in this field. W Chen et al. [6] have established a comprehensive dynamic model which involves voltage, gas supply and temperature dynamic model, and validated by physical monitoring platform. A D Le et al. [7] have studied a general PEMFC model which is three-dimensional and focused on liquid water effects on the performance of cell by CFD software. Recently, X Lei et al. [8] have described a two-dimensional PEMFC model that coupled with liquid water and gas, and analyzed the cell performance by the function current density.

According to the above description, most of the models are usually adopted to simulate the steady-state and dynamic variations. However, it is essential to study the influence of control strategies on cell dynamic response. Some scholars have also made contributions to this field. RN Methekar et al. [9] have proposed the linear ratio controller to control the flow rate of oxygen. They found that this control strategy provides more superior dynamic response and decreases the solid temperature. J Luna et al. [10] have designed a nonlinear model predictive controller that based on the distributed parameters PEMFC model. What they found is that the efficiency and durability of the system are enhanced observably.

At present, the output voltage control strategies of fuel cell are mainly PID control, sliding mode variable structure control, fuzzy control, neural network control and some other intelligent control strategies. The sliding mode variable structure control system has the advantages of fastness, no overshoot, small computation, real-time and so on [11-12]. However, the discontinuity of the variable structure control and the frequent switching of the controller may cause the tracking error, produce the chattering phenomenon near the zero point and it can't be eliminated. The important feature of the fuzzy control is to simplify the control algorithm [13]. But it lead to the design of the fuzzy controller is not a unified design criteria and is arbitrary. Neural network control mainly deals with the control problem of complex nonlinear, uncertain and unknown systems which can't be solved by traditional technology [14]. However, neural network control has the problem of self-learning. When the environment changes, the original mapping is no longer applicable and need to re-training network. PID controller has a good physical meaning, easy to adjust parameters, to achieve a simple, robust and other advantages in the automatic control system has been dominated. The PID controller has the advantages of clear physical meaning, easy parameter adjustment, simple implementation and strong robustness. It has been in a dominant position in the automatic control system. The control object of this paper is the PEMFC system, which is a highly nonlinear and time-varying system. In order to realize the high performance of the system, based on the traditional integer order PID control, the fractional calculus theory is used to improve the control quality of the integer order PID. It is expected to integrate and carry forward the advantages of traditional PID controller and be able to make up for its shortcomings at the same time.

Recently, the fractional order $PI^{\lambda}D^{\mu}$ (FOPID) controller has been received considerable attention in the past decade, in which the order of differential and integral is fractional. With the

FOPID controller proposed in the 1990s [15], the application of fractional calculus has gradually penetrated from theoretical research into many engineering applications. In [16] it is used for designing aerospace control systems, in [17] for autonomous micro grid system, and in [18-19] for automatic voltage regulator system. In the field of fuel cell, fractional calculus theory is widely used in fuel cell modeling [20-21].

In the fractional order control system simulation analysis and practical application, it is necessary for the fractional order calculus operator s^r ($r \in \mathrm{R}$) to be approximated as the integer order by the digital implementation algorithms. At present, the digital implementation algorithms mainly includes [22-25]: short memory method based on G-L definition, PSE expansion method, CFE expansion method and Oustaloup filter method.

It is found that the Oustaloup filter method is the best one in the digital implementation algorithms, but the Oustaloup method is not very effective at both ends of the approximation frequency domain. In order to ensure the accuracy and practicability in the whole approximate frequency domain, the method of [26] is proposed to improve the Oustaloup filter method in this paper. The improved Oustaloup filter algorithm has higher amplitude-frequency characteristics and approximation accuracy of phase-frequency characteristics in the frequency domain, and its structure is also convenient to implement the fractional-order system block diagram.

It is undeniable that the satisfactory results would be obtained if the FOPID control is applied to control the PEMFC output voltage under varying load conditions. But it is not up to the requirements of real-time control. Besides, it would be found that simulation time is too short to system operation. As a result, this paper develops a real-time PEMFC virtual test system which integrates Labview and Matlab/simulnk with simulation interface toolkit (SIT) sever. K Senthilnathan et al. [27] have established the monitoring system by SIT sever to analyses the performance of UPQC system. The impact of the load fluctuation on the system can be clearly seen on the monitoring window. K Hu et al. [28] have developed a real-time transform system of spray volume that based on the Labview and Matlab/simulink. With respect to the traditional system, it can transfer data in high speed and program in less complexity. At present, most of the fuel cell test systems are based on the fuel cell experimental platform and industrial computer. While the PEMFC test system designed in this paper is based on the fuel cell Simulink model and Labview simulation interface toolkit, which can get better effect in verifying the effectiveness of the control algorithm and monitoring the process of the system with minimal cost.

In summary, the FOPID controller that adopts the improved Oustaloup filter algorithm was applied to control the hydrogen inlet pressure of the PEMFC system. The performance was compared with that of PID control. It was found that the FOPID controller had better dynamic performance and improved the system efficiency. In the meantime, the real-time test system made the problems that the previous control strategy could only realize off-line control and high cost of implementing real-time simulation with hardware-in-the-loop solved. The results of this paper provide an experimental method and theoretical basis for the application of PEMFC robot and the establishment of its measurement and control platform.

2. THE LUMPED PARAMETER MODEL OF THE PEMFC

2.1 The principle of the PEMFC

The main components of the PEMFC include electrode, proton exchange membrane, bipolar plate and gas flow. The hydrogen is decomposed into hydrogen ions and electrons under the action of the anode catalyst (Eq. (1)). At this point, the hydrogen ions get through the proton exchange membrane into the cathode and the electrons flow through the external circuit, so as to reach the cathode. Under the action of the cathode catalyst, the oxygen reacts with hydrogen ions and electrons to form water (Eq. (2)) and release some of the heat. Water management is in the form of discharge of most water. The remaining water spreads to the anode through proton exchange membrane by the pressure difference. The total reaction is shown in Eq. (3).

Anode reaction: $H_2 \rightarrow 2H^+ + 2e^-$, (1)

Cathode reaction: $\frac{1}{2}O_2 + 2H^+ + 2e^- \rightarrow H_2O$, (2)

Overall reaction: $\frac{1}{2}O_2 + H_2 \rightarrow H_2O + heat$. (3)

2.2 The model of the PEMFC

The lumped parameter of PEMFC is just related to the reaction time and has nothing to do with the space. In this paper, a dynamic model of multi-input and multi-output is established. The following assumptions should be made before modeling,

(i) Reactant gas is ideal and evenly distributed.

(ii) The gas entering the flow field can be well humidified.

(iii) The PEMFC works under 100℃.

(iv) The control equipment outside the cell runs well.

(v) The process of gas flow is one-dimensional.

Under the standard condition, the theoretical potential of the monolithic PEMFC is 1.229V, which represents all of the chemical energy of the fuel is converted into electromotive force. However, the fuel cell reaction is irreversible. The actual electromotive force is lower than the theoretical, which is usually referred to the “polarization overvoltage”. There are three kinds of polarization which lead to irreversible loss: (i) activation polarization; (ii) ohmic polarization; (iii) concentration polarization. Therefore, the stack voltage of the PEMFC is shown in Fig.1.

In the course of normal operation, there exists a phenomenon of “double-layer charge” in the PEMFC stack. That is, the hydrogen ions accumulate on the surface of the electrolyte, while the electrons accumulate on the surface of the electrode, which causes a voltage difference between them and as a capacitor in circuit. When the current is changed, the activation overvoltage and the concentration overvoltage need to be delayed for some time to respond to the current output voltage [29]. A parallel capacitor can be used in the circuit to indicate the influence of the double layer charge.

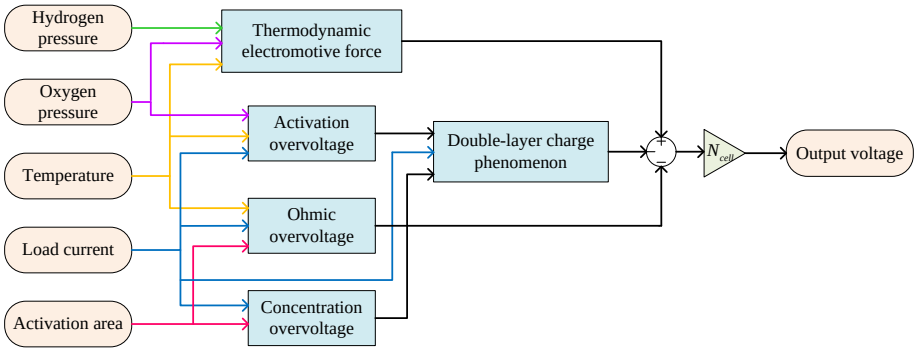

Figure 1. The stack voltage schematic diagram of PEMFC

When the load current I is in steady state, the capacitor C has no charge/discharge process. So, the capacitor voltage U_c is equal to the sum of the voltage of R_{act} and R_{conc}, which is calculated by

$$U_c = I\left(R_{act} + R_{conc}\right), \tag{4}$$

Where, R_{act} and R_{conc} denote the equivalent resistance of the activation loss and the concentration loss respectively, I is the steady state current before the load changes, and U_c is the voltage of the equivalent capacitor under the influence of double-layer charge.

In steady state, the output voltage of the single fuel cell is described as

$$U_{out} = E_{nernst} - U_c - I \times R_{ohm}. \tag{5}$$

where E_{nernst} is the thermodynamic electromotance in PEMFC, R_{ohm} denotes the equivalent resistance of ohmic loss, U_{out} is the output voltage of single in steady state.

When the load changes suddenly, the capacitor C is charging or discharging. At this moment, the capacitor voltage u_c can be described as

$$u_c = \left(R_{act} + R_{conc}\right)\left(I_L - C\frac{du_c}{dt}\right), \tag{6}$$

where u_c denotes the capacitor voltage and I_L is the feedback current after the load changes suddenly.

The instantaneous voltage value of capacitance C can be obtained by the Laplasse transform of the Formula (6), that is

$$u_c(t) = \left(\frac{I_L}{C} - \left(R_{act} + R_{conc}\right)I\right)\exp\left(-\frac{1}{\left(R_{act} + R_{conc}\right)C}\right). \tag{7}$$

When the load is changed suddenly, the output voltage of the single fuel cell is described,

$$u_{out}(t) = E_{nernst} - u_c(t) - I_L \times R_{ohm}. \tag{8}$$

2.3 Determination of the parameters

E_{nernst} expression is as follow

$$E_{nernst} = \frac{\Delta G}{2F} + \frac{\Delta S}{2F}\left(T - T_{ref}\right) + \frac{RT}{2F}\left[\ln\left(P_{H_2}\right) + \frac{1}{2}\ln\left(P_{O_2}\right)\right]. \tag{9}$$

Where, ΔG is the change of the Gibbs free energy, F is the Faraday constant, ΔS is the change of the entropy, R is the ideal gas constant, P_{H2} and P_{O2} are the partial pressure of hydrogen and oxygen

respectively, and T and T_{ref} are the actual temperature and reference temperature of the fuel cell respectively.

R_{act} is related to the current density and the cell temperature, which mainly works in the low current density region and increases with the temperature rising.

$$R_{\mathrm{act}} = \frac{V_{act}}{I} = \frac{\xi_1 + \xi_2 T + \xi_3 T \ln\left(C_{O_2}\right) + \xi_4 T \ln\left(I\right)}{I}, \tag{10}$$

$$C_{O_2} = \frac{P_{O_2}}{5.08 \times 10^6 \exp\left(-498 / T\right)}. \tag{11}$$

Where ξ_i (i=1,2,3,4) are the empirical parameters, and C_{O2} is the oxygen concentration of the gas-liquid interface.

The parameters of PEMFC is shown in Table.1.

Table 1. The parameters of the PEMFC

Symbol	Physical meaning	Value
N_{cell}	the number of cells	545
T	the temperature of PEMFC stack (K)	353.15
T_{ref}	the reference temperature (K)	298.15
F	the Faraday constant (C/mol)	96485
R	the ideal gas constant (J/K•mol)	88.314
ΔS	the change value of entropy (J/mol)	-164.0279
ΔG	the change value of Gibbs energy (J/mol)	237180
R_C	the electron flow impedance (Ω)	0.0048
C	the equivalent capacitor of double-layer charge (F)	3
ξ_1	the empirical parameter	-0.9514
ξ_2	the empirical parameter	0.00312
ξ_3	the empirical parameter	7.4×10^{-3}
ξ_4	the empirical parameter	1.87×10^{-4}
A	the activation area of single cell (cm^2)	50
l	the thickness of exchange membranes (μm)	51
h	the humidity of the exchange membranes	20
B	the working constant	0.016
J_{max}	the maximum current density (A/cm^2)	1.5

R_{ohm} is composed of the equivalent membranes impedance R_m and the impedance R_C that impede the proton getting through the membranes. According to the resistivity theorem, the equivalent membrane impedance R_m can be described as

$$R_m = \frac{r_m l}{A}, \tag{12}$$

Where A is the activation area, l is the thickness of exchange membranes, r_m is the resistivity of exchange membranes. It is therefore possible to formulate r_m as follow [29]

$$r_m = \frac{181.6\left[1+0.03\left(\frac{I}{A}\right)+0.062\left(\frac{T}{303}\right)^2\left(\frac{I}{A}\right)^{2.5}\right]}{\left[h-0.634-3\left(\frac{I}{A}\right)\right]\exp\left(4.18\left(\frac{T-303}{T}\right)\right)}. \tag{13}$$

Where h is the water content of the exchange membranes.

The concentration loss acts mainly occurs in the high current density region, which results in the decrease of the pressure of the cathode and anode in the electrochemical reaction. The equivalent resistance of the concentration loss R_{conc} is described as

$$R_{conc} = -\frac{B}{I}\ln\left(1-\frac{J}{J_{\max}}\right). \tag{14}$$

Where B is the working constant of the PEMFC, J is the actual current density and J_{max} is the maximum current density.

The output voltage, output power, consumption power and efficiency of the PEMFC stack are as follows

$$\begin{cases} U_{stack} = N_{cell} \times U_{out} \\ P_{stack} = U_{stack} \times I \\ P_{con} = N_{cell} \times I^2 \left(R_{act} + R_{conc} + R_{ohm}\right) \\ \eta = \dfrac{U_{out}}{E_{nernst}} \end{cases} \tag{15}$$

2.4 Model validation

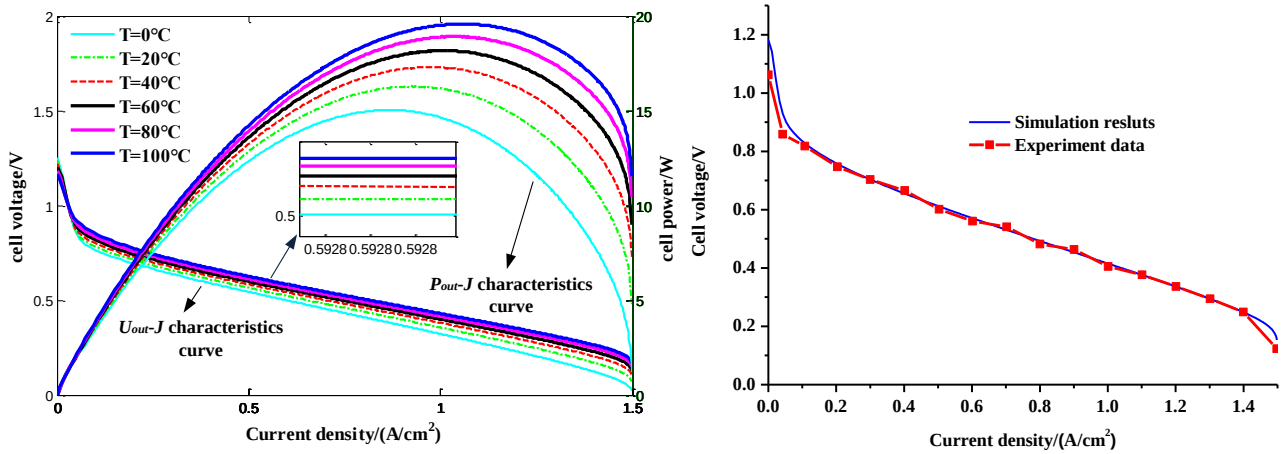

(a) Electrical characteristics of different temperature (b)U_{out} - J characteristics in case of T=80℃

Figure 2. Electrical characteristics of single cell

The PEMFC dynamic model is validated in MATLAB and experiment environment. The unit ramp function is taken as the load current, and both the oxygen and hydrogen pressures are set to 1 atm. Fig.2 (a) shows the current density-voltage and current density-power when a single cell runs at different temperature. As the temperature increases, the output voltage of fuel cell increases

accordingly. However, the operating temperature range of the PEMFC is limited by the proton exchange membrane. The excessive high temperature will cause the proton exchange membrane to lose water and reduce the ability of conducting protons. Therefore, the PEMFC operating temperature is generally maintained at about 80℃, and the maximum power point is around the current density of 1.05 A/cm^2 at this temperature. The experiment had been done by the G200 fuel cell test equipment (Green Innovation Company). The experiment data were fitted by the software to obtain the current density- cell voltage comparison figure of the experiment data and simulation results, which is shown as Fig.2 (b). It can be seen in the figure, in case of low current density, there are some deviations between simulation results and experiment data. It mainly caused by the formulas had been simplified when establishing the PEMFC model. But the deviations is basically within the error range. In other cases, the experiment results agree well with simulation results, which proves the effectiveness and correction of the PEMFC model.

3. FOPID CONTROLLER DESIGN

The FOPID controller has two more adjustable parameters than PID controller, and the order of the controller can be chosen arbitrarily, so the FOPID controller owns more flexibility. In addition, the FOPID controller has great adaptability to the parameter variation of the control system. When the parameters of the control system change within a certain range, the system characteristics remain unchanged, so the FOPID controller has the characteristic of strong robustness. While the PEMFC is a highly nonlinear, large time-delay system and the actual conditions are more complex. For such a system, the system responses slowly and control accuracy is not high after adopting the conventional control algorithm. In order to ensure the fast response and stability of the output voltage of the PEMFC system, the FOPID control method is applied to control the output voltage of PEMFC under varying load conditions.

3.1 Fractional calculus

Fractional calculus is the succession and development of the integer order calculus. Which has any order. The general expression of the fractional calculus is [30]

$$ {}_{\alpha}D_t^{\alpha} f(t) = \begin{cases} \dfrac{d^{\alpha}}{dt^{\alpha}} f(t), \mathrm{Re}(\alpha) > 0 \\ f(t), \mathrm{Re}(\alpha) = 0 \\ \int_{\alpha}^{t} f(\tau)(d\tau)^{-\alpha}, \mathrm{Re}(\alpha) < 0 \end{cases}, \tag{16} $$

Where, ${}_{\alpha}D_t^{\alpha}$ is the calculus operator and α is any real number or plural.

Different mathematicians give the different definitions of the fractional calculus. In the control field, the Riemann-Liouville's definition is more often widely used than other definitions, and its expression is

$$ {}_{\alpha}D_t^{\pm\alpha} f(t) = \frac{1}{\Gamma(n-\alpha)} \left(\frac{d}{dt}\right)^n \int_{\alpha}^{t} \frac{f(\tau)}{(t-\tau)^{\alpha-n+1}} d\tau, \quad (17) $$

where n-1<α<n (n∈N) and Γ represents the Gamma function given by

$$ \Gamma(z) = \int_0^{\infty} e^{-t} t^{z-1} dt, \quad (18) $$

According to the R-L definition, the Laplace transform in Eq. (17) is given below

$$ L\left[{}_{\alpha}D_t^{\alpha} f(t)\right] = s^{\alpha} F(s) - \sum_{k=0}^{n-1} s^{\alpha-k-1} f^{(k)}(0). \quad (19) $$

3.2 The Controller structure based on FOPID

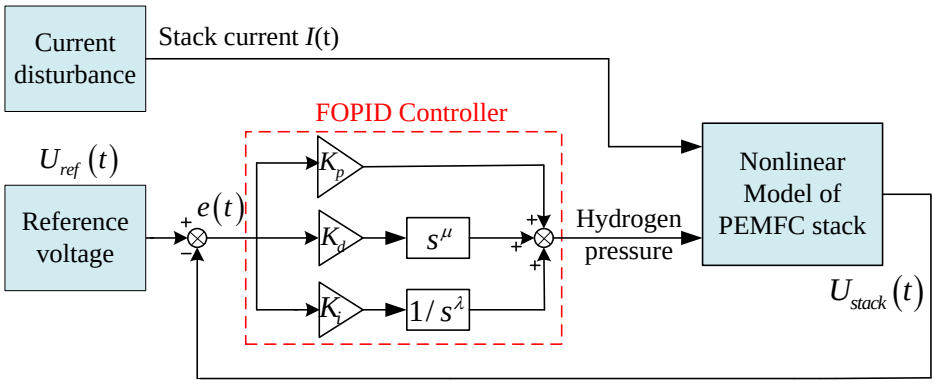

Figure 3. The control structure block diagram of PEMFC system

The mathematical model of the FOPID controller can be drawn as follows

$$ u(t) = K_p e(t) + K_i D^{-\lambda} e(t) + K_d D^{\mu} e(t) \quad (20) $$

$$ C(s) = K_p + K_i s^{-\lambda} + K_d s^{\mu}, 0 < \lambda, \mu < 2 \quad (21) $$

Where the Eq. (20) is the time domain model and the Eq. (21) is the frequency domain model.

The FOPID control structure of the PEMFC system is shown as Fig.3. U_{ref}(t) is the system reference voltage, U_{stack}(t) is the actual system output voltage, I_L(t) is the stack feedback current after the load changes suddenly, and *e*(t) is the error signal between reference voltage and the actual voltage. The error signal controlled by FOPID is used as the input signal of hydrogen pressure.

3.3 FOPID controller digital implementation

The fractional order calculus is related to all the information in the past, which makes the fractional integral and differential equation solving process more complex than the integer order. Therefore, the calculus operator s^r needs to be fitted by numerical calculation and fractional discretization in the simulation and engineering applications. An improved Oustaloup filter algorithm is used to calculate the unknown signal by fractional calculus.

The calculus operator s^r is usually fitted to approximate the integer order by the Oustaloup filter algorithm in frequency domain, but the approximation effect at the ends of approximate

frequency is not efficient. The improved Oustaloup filter algorithm introduces the appropriate weight coefficients *b* and *d* in the approximation process to get much better effect.

Assuming that the frequency range is limited to (ω_b, ω_h), the fractional calculus operator s^r can be approximated by the following transfer function

$$K(s)=\left(\frac{1+\frac{s}{d\omega_b/b}}{1+\frac{s}{bs\omega_h/d}}\right)^r, \tag{22}$$

Where, 0< r <1, s= jω, b> 0, d> 0.

The simplified formula of $K(s)$ is as follows

$$K(s)=\left(\frac{bs}{d\omega_b}\right)^r\left(1+\frac{-ds^2+d}{ds^2+bs\omega_h}\right)^r, \tag{23}$$

In the frequency domain of $\omega_b < \omega < \omega_h$, the Taylor series is used for transfer function expansion.

$$K(s)=\left(\frac{bs}{d\omega_b}\right)^r\left(1+rp(s)+\frac{r(r-1)}{2}p^2(s)+\cdots\right), \tag{24}$$

Where

$$p(s)=\frac{-ds^2+d}{ds^2+bs\omega_h}. \tag{25}$$

Combining the Eq. (22) and Eq. (24),

$$s^r=\frac{(d\omega_b)^r b^{-r}}{\left(1+rp(s)+\frac{r(r-1)}{2}p^2(s)+\cdots\right)}\left(\frac{1+\frac{s}{d\omega_b/b}}{1+\frac{s}{b\omega_h/d}}\right)^r, \tag{26}$$

The first order term of Taylor series in Eq. (26) is preserved and replaced with Eq. (25),

$$s^r=\left(\frac{d\omega_b}{b}\right)^r\left(\frac{ds^2+bs\omega_h}{d(1-r)s^2+bs\omega_h+dr}\right)\left(\frac{1+\frac{s}{d\omega_b/d}}{1+\frac{s}{b\omega_h/d}}\right)^r. \tag{27}$$

As can be seen form formula (27), there are three poles, they are

(i) One of the poles is at $-b\omega_h/d$, and the pole lies on the negative half axis of the s-plane when ω_h> 0, *b*> 0, *d*> 0.

(ii) The other two poles are the roots of the Eq. (28). When 0<r<1, the real part of the root of the equation is negative, so the two poles lie on the negative half plane of S.

$$d(1-r)s^2+b\omega_h s+dr=0 \tag{28}$$

It can be concluded that s^r is stable within the frequency range (ω_b,ω_h).

The irrational fractional part of Eq. (27) can be approximated by the following rational model

$$K(s)=K\left(\frac{ds^2+bs\omega_h}{d(1-r)s^2+bs\omega_h+dr}\right)\prod_{k=-N}^{N}\frac{1+\frac{s}{\omega_k'}}{1+\frac{s}{\omega_k}}, \tag{29}$$

and the zero and pole of rank *k* can be described as

$$\omega_k' = \left(\frac{b}{d}\right)^{\frac{2k-r}{2N+1}} \omega_h^{\frac{N+k+\frac{1}{2}(1-r)}{2N+1}} \omega_b^{\frac{N-k+\frac{1}{2}(1+r)}{2N+1}}, \tag{30}$$

$$\omega_k = \left(\frac{b}{d}\right)^{\frac{2k+r}{2N+1}} \omega_h^{\frac{N+k+\frac{1}{2}(1+r)}{2N+1}} \omega_b^{\frac{N-k+\frac{1}{2}(1-r)}{2N+1}}, \tag{31}$$

Where

$$K = (\omega_b \omega_h)^r. \tag{32}$$

According to the analysis about the fractional order approximation operator s^r, the controller design steps are as follows:

Step.1 Determine the fitting parameters: the approximation frequency (ω_b, ω_h), the weight coefficient *b*, *d* and the filter order *N*.

Step.2 Determine the controller parameters: K_p, K_i, K_d, the integral order λ and differential order μ.

Step.3 Calculating the corresponding rational approximation transfer function $K_1(s)$ and $K_2(s)$, which is correspond to the integration operator $s^{-\lambda}$ and differential operator s^{μ}.

Step.4 Calculating the rational approximate transfer function C (s) of the FOPID controller, which can be obtained by the following formula.

$$C(s) = K_p + K_i K_1(s) + K_d K_2(s). \tag{33}$$

3.4 The fitting effect analysis

To analysis the fitting effect of the operator $s^{0.5}$ by using the improved Oustaloup algorithm, the relevant parameters are determined with the approximate frequency range (10^{-5},10^{3}), the weight coefficient *b*=10, *d*=9 and the filter order *N*=3. The Bode diagram of $s^{0.5}$ is shown in Fig.4, which are the results of adopting two different methods.

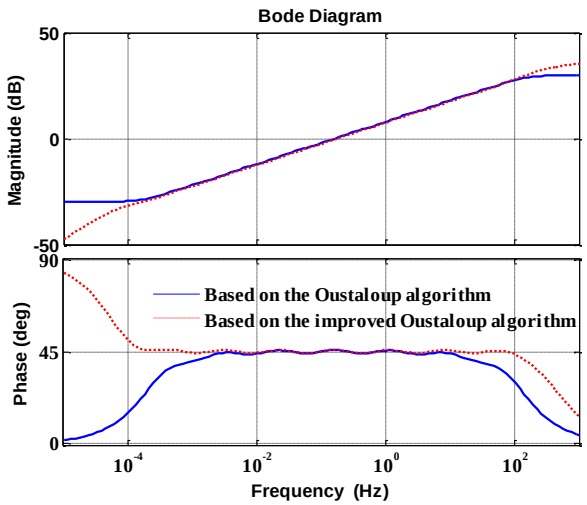

Figure 4. Comparison of $s^{0.5}$ Bode diagram

As we all know, the pure differential is an oblique line on the Bode amplitude-frequency characteristic, and a horizontal line on the Bode phase-frequency characteristic. For the differential operator $s^{0.5}$, the transfer function is

$$G(s) = s^{0.5}. \tag{34}$$

The frequency expression of Eq. (34) is

$$G(\omega) = (j\omega)^{0.5}. \tag{35}$$

Theoretically, the amplitude-frequency and phase- frequency expressions of $s^{0.5}$ are as follows

$$A(\omega) = |G(j\omega)| = \omega^{0.5}, \tag{36}$$

$$\varphi(\omega) = \angle G(j\omega) = 45^{\circ}, \tag{37}$$

and the logarithmic frequency expression is

$$L(\omega) = 20\lg A(\omega) = 10\lg \omega. \tag{38}$$

As can be seen from Fig.4, the fitting effect of the Oustaloup algorithm at the boundaries is not satisfactory, especially the distortion degree of the phase is more serious. While the improved Oustaloup algorithm maintains good accuracy in the frequency range. Therefore, this paper uses the improved Oustaloup algorithm to obtain the fractional order operator module by encapsulating the calculus operator. The parameters of the controller can be easily changed through the module.

4. THE DEVELOPMENT AND DESIGN OF REAL-TIME TEST SYSTEM

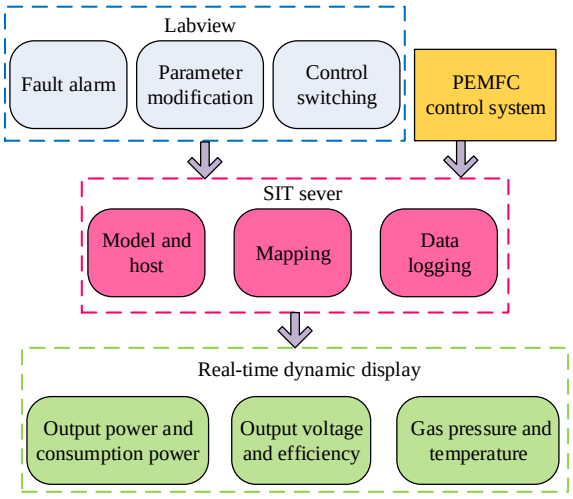

Figure 5. Flow chart of co-simulation

The FOPID control method is not up to the requirements of real-time control. Besides, it would be found that simulation time is too short to system operation. Therefore, a real-time virtual test system is developed which integrates Labview and Matlab/simulnk with simulation interface toolkit sever.

In order to test the PEMFC control conveniently, the test system features are designed as follows

(i) The FOPID control and PID control can be switched freely and prompted by the green light, so as to observe the difference between them.

(ii) The reference output voltage, the stack operating temperature, the cells number and the controller parameters of the system can be modified in real time.

(iii) The output voltage, the output power, the power consumption, the system efficiency and the bipolar gas pressure of the PEMFC system can be displayed in real time.

(iv) The red lights will be on if the reactor temperature, hydrogen pressure, oxygen pressure and load current exceed the threshold respectively.

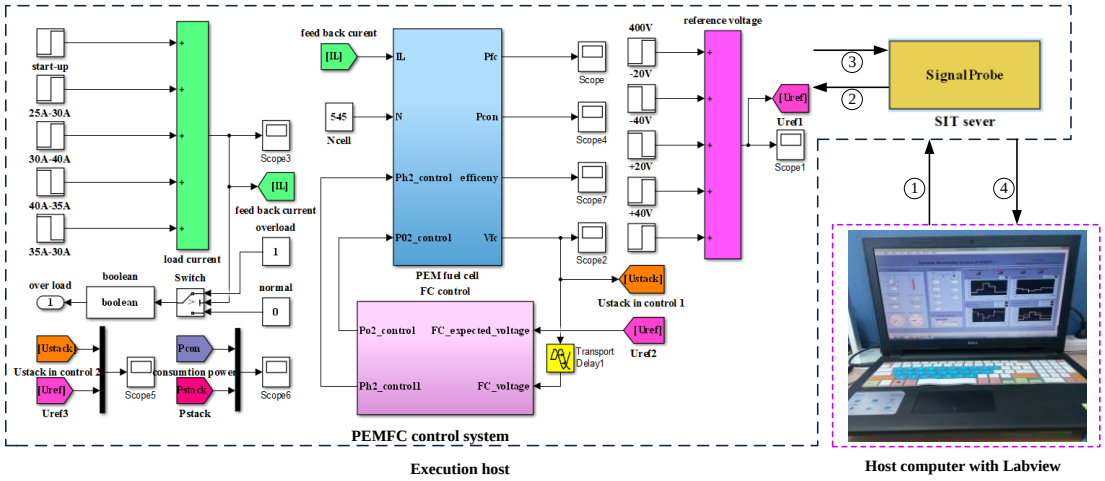

Figure 6. The PEMFC real-time test system

According to the above test system features, the flow chart of the PEMFC virtual real-time test system is shown in Fig.5. Firstly, a model of PEMFC control system must be established in Simulink. Secondly, configuring the parameters of SIT dialog box and completing the mappings between the PEMFC model and monitoring interface. Finally, the control and cell parameters input and simulation data output can be realized interactively for monitoring the PEMFC operation status and dynamic characteristic of the control effect in real-time.

At last, the structure of PEMFC real-time test system is shown in Fig.6. It mainly includes the PEMFC control system as the executive mechanism and host computer as the monitoring mechanism. Among them, the executive mechanism is related to the establishment of the PEMFC lumped parameter model, the controller design and the disposition of SIT sever parameter; the monitoring mechanism is focused on developing the monitoring contact surface.

When the user want to change the parameters of the controller or PEMFC through the monitoring interface, the SIT sever performs the following steps corresponding to the label in Fig.6.

Step.1 The front panel of Labview sends the updated data to the SIT sever by using transmission control protocol/ internet protocol (TCP/IP) communication network.

Step.2 When the SIT parameters are configured, the updated data will be passed to the PEMFC control system.

Step.3 The system runs according to the new parameters and outputs the updated signal value. At the same time, the SIT sever detects the output signals of the PEMFC model automatically which has established the relevant mapping condition.

Step.4 The SIT server passes the updated output signal to the Lavbview front panel, where the relevant indicator on the front panel responds actively.

5. RESULTS AND DISCUSSION

In order to verify the advantages of the designed FOPID control that adopts the improved Oustaloup algorithm in the PEMFC control system, the comparisons between FOPID and PID on the dynamic output characteristic of PEMFC will be discussed.

5.1 System test in Labview

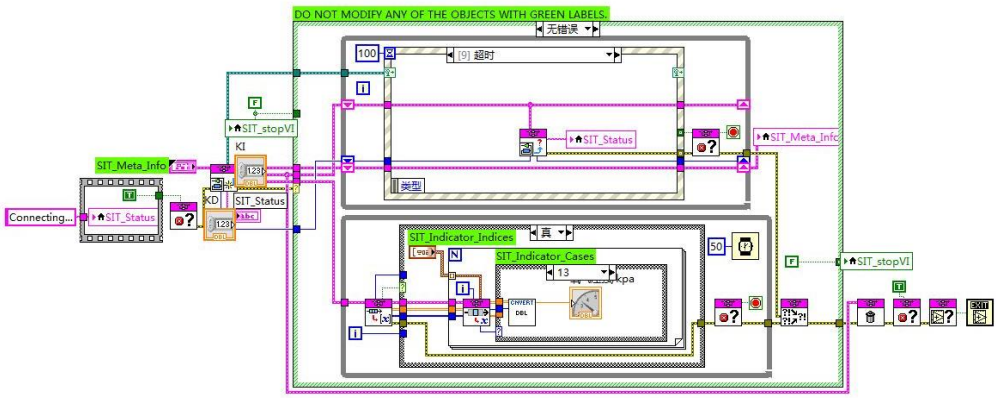

Figure 7. Block diagram for connecting the Labview and SIT server

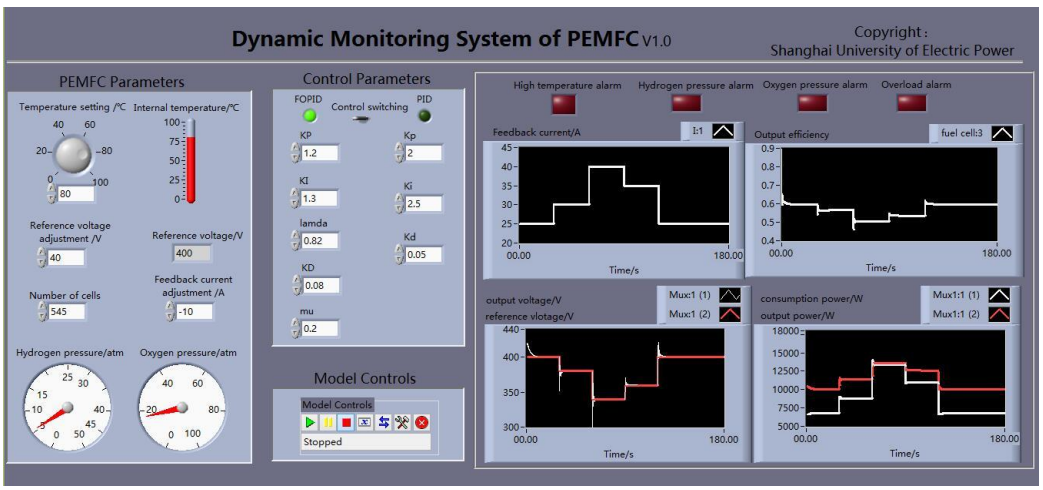

Figure 8. The results of the PEMFC test system in Labview

The PEMFC control system is a typical non-linear and time-varying system, so it can't be expressed by a definite transfer function. For such a complex system, the test system designed in this paper can be used to adjust the controller parameters visually to determine the effect of the FOPID controller and the PID controller. Finally, the FOPID controller and PID control transfer functions are determined respectively as follows

$$C_1(s) = 1.2 + 1.3\frac{1}{s^{0.82}} + 0.08s^{0.2}, \tag{39}$$

$$C_2(s) = 2 + 2.5\frac{1}{s} + 0.05s. \tag{40}$$

The performance analysis and monitoring of the PEMFC control system is done by the real-time test system. The analysis of the PEMFC control system based on the PEMFC lumped parameter model under the various conditions is performed. The performance monitoring is done with the interfacing of the simulation model with the SIT sever, which is connected through the TCP/IP communication network. The advantage of this real-time test system is that, we can monitor the performance of the PEMFC control system with a single panel and we can also analyze the working status under the various disturbances. Fig.7 shows the block diagram for the connection to SIT server and Labview. And the visual results of the real-time test system which based on the determined controller parameters is shown in Fig.8.

5.2 Comparison and discussion about the control performance

The load current shown in Fig.9 is selected as the input of the system, and the task of the controller is to complete the reference voltage tracking control shown in Fig.9. Thus, the dynamic output voltage response of the PEMFC system is shown in Fig.10. In the case of abrupt change of external load, both control strategies can stabilize the output voltage of the PEMFC near the corresponding reference voltage; in the stable interval, the output voltage fluctuation of FOPID is smaller than that of PID. It's favorable for the PEMFC system in the long-term stable operation.

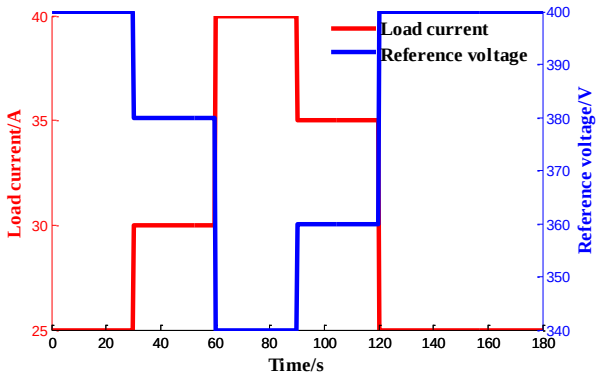

Figure 9. Change of the load current and the reference voltage

The PEMFC control system performance indicators under the two control methods is shown in Fig.11. When the PEMFC system runs in the process of start-up, 25A-30A, 30A-40A, 40A-35A, and

35A-25A, compared with the PID control method, the FOPID control method reduces the overshoot of the PEMFC system by 2.88%, 5.78%, 14.8%, 0.76% and 1.2% respectively. What's more, the settling time of the system is shortened by 0.84s, 2.2s, 0.7s, 0.12s and 0.2s respectively. From the concussion number in the Fig.11, we can see the FOPID controller has good robustness and anti-jamming in the PEMFC system. This method can effectively avoid the effect of output performance and service life caused by the high overshoot of the system. In addition, it can also reduce the settling time of the system and is conducive to the long-term high efficiency and stability of the PEMFC system.

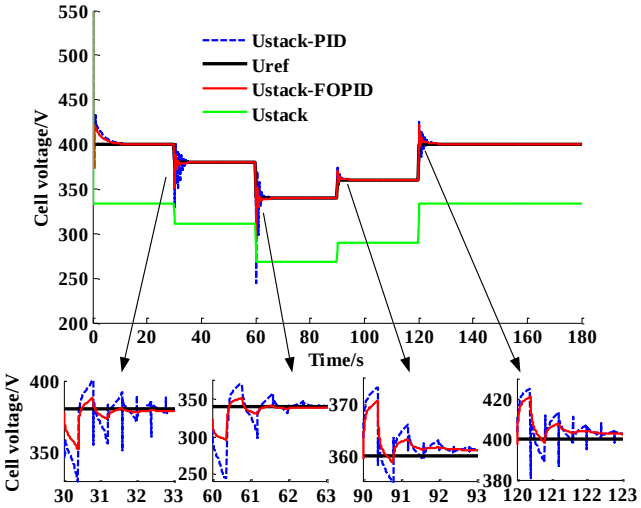

Figure 10. PEMFC output voltage response under different control method

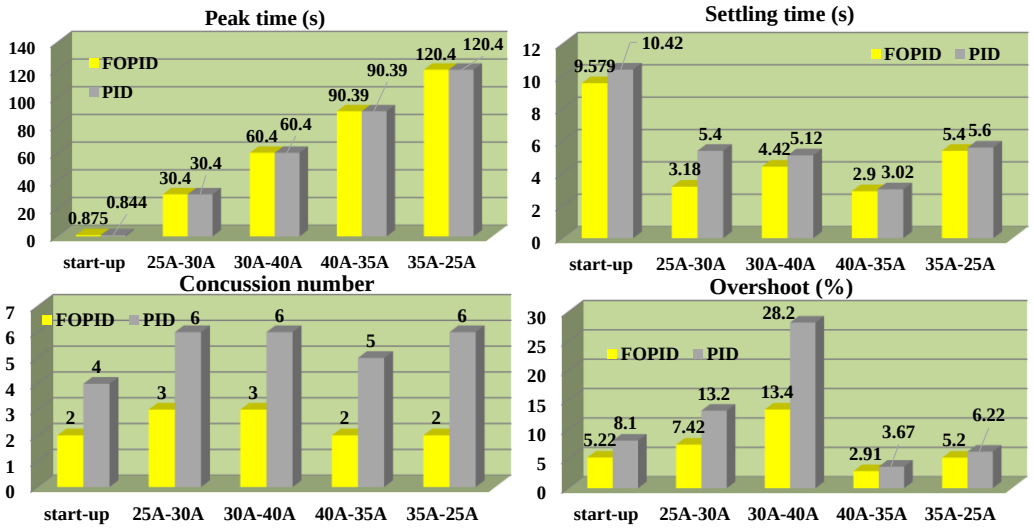

Figure 11. The control performance comparison in the PEMFC control system

Fig.12 (a) depicts the variation of consumption power and output power in the PEMFC control system. In order to compare the power characteristic of the PEMFC system under the two control

methods, the output power and consumption power under the FOPID control are subtracted from that under the PID control respectively to obtain the power error curve between the two control methods shown in Fig.12 (b). From Fig.12 we can see that, in the case of a sudden change of external load, both control methods can stabilize the actual system output power near the desired output power. While compared with the FOPID control, the consumption power of the PEMFC system under the PID control is increased by about 200W. Thus, it can be seen from Fig.13 that the system efficiency is improved by about 0.6% after adopted the FOPID control.

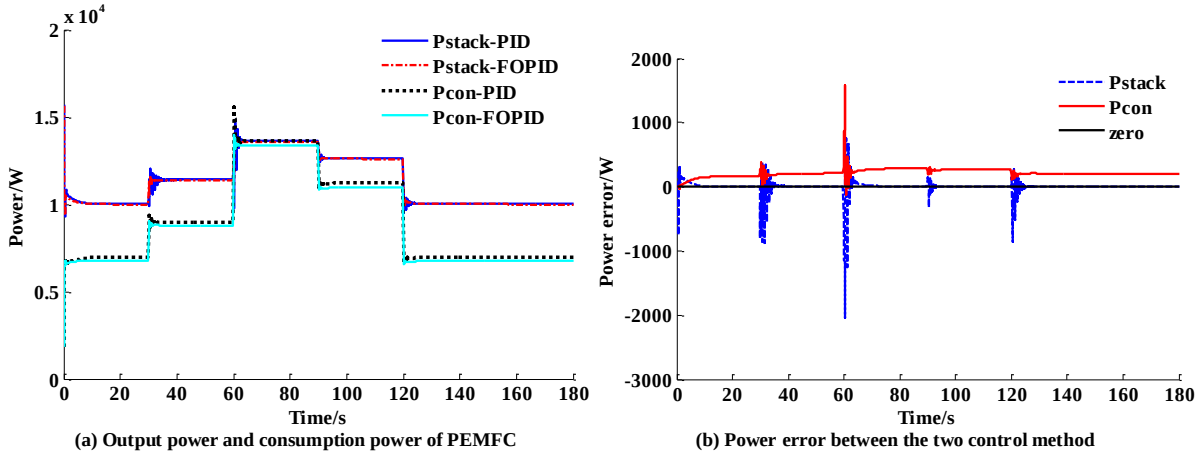

Figure 12. PEMFC power response under different control method

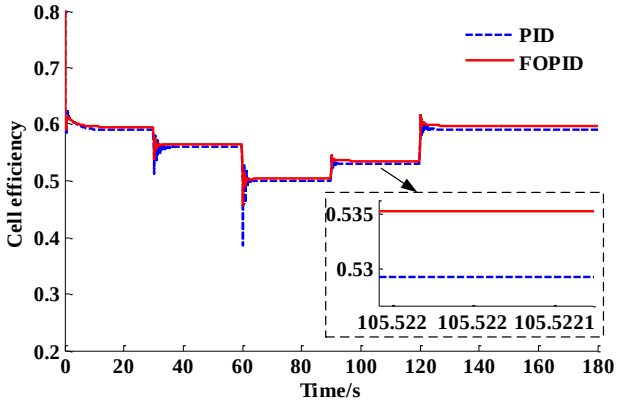

Figure 13. Efficiency of PEMFC system

In the traditional control theory, almost all the control systems are described by the differential equations which the differential is considered as the integer. In fact, there are many physical systems that exhibit the fractional order dynamics due to their special materials and chemical properties. The Ref. [31] shows that the actual system is usually a fractional order, and it is better to reveal the essential characteristics of the object and it behavior when using the fractional order to describe those objects with fractional characteristics. The FOPID controller has two more adjustable parameters than PID controller that are λ and μ, and the order of the controller can be chosen arbitrarily, so the FOPID

controller owns more flexibility. In addition, the FOPID controller has great adaptability to the parameter variation of the control system.

6. CONCLUSION

The FOPID controller that adopts the improved Oustaloup algorithm is applied to the PEMFC control system. The proposed FOPID controller effectively decreases the settling time and the overshoot of the PEMFC system and improves the system efficiency, which increases the utilization of hydrogen greatly and completes the purpose of saving energy. In addition, the FOPID controller is robust to changes in PEMFC system parameters. Moreover, the real-time test system that integrates the PEMFC simulink model and Labview monitoring interface with SIT sever can monitor the running status of the system and verify the correctness of the control algorithm. And the monitoring interface designed by Labview has the advantages of high reliability and visualization. In the future, it is valuable to consider the synchronous management of electrical and thermal energy of PEMFC system.

ACKNOWLEDGMENTS
The authors would like to thank the National Natural Science Foundation of China (Grant No. 51405286) and Shanghai Key Laboratory Power Station Automation Technology Laboratory (Grant No.13DZ2273800) for financial support towards this research.

References

1. X. Lü, K. Zhang, Y. Wu, *Int. J. Adv. Manuf. Technol.*, 88 (2017) 2201.
2. L. Valverde, F. Rosa, C. Bordons, *IEEE Trans. Ind. Inform.*, 9 (2013) 1398.
3. J. E. Larminie, A. L. Dicks, *J. Power Sources.*, 84 (2013) 194.
4. S. M. Hosseini, A. H. Shamekhi, A. Yazdani, *J. Renew. Sustain. Ener.*, 4 (2012) 043107.
5. V. Mehta, J. S. Cooper, *J. Power Sources.*, 114 (2003) 32.
6. W. Chen, H. Zhang, Q, Li, *J. Southwest. Jiaotong. Univ.*, 47 (2012) 1003.
7. A. D. Le, B. Zhou, *J. Power Sources.*, 182 (2008) 197.
8. X. Lei, S. Du, R. Chen, M. Mamlouk and K. Scott, *Energy.*, 96 (2016) 80.
9. R. N. Methekar, V. Prasad, R. D Gudi. *J. Power Sources.*, 165 (2007) 152.
10. J. Luna, S. Jemei, N. Yousfi-Steiner, A. Husar and M. serra, *J. Power Sources.*, 328 (2016) 250.
11. G. Park, Z. Gajic, *J. Power. Sources.*, 212 (2012) 226.
12. G. Park, Z. Gajic, *IEEE Trans. Energy. Conver.*, 29 (2014) 65.
13. S. W. Tong, D. W. Qian, *Int. J Hydrogen. Energ.*, 38 (2013) 4124.
14. S. A. Hajimolana, M. A. Hussain, W. M. A. W Daud and M. H. Chakrabarti, *Int. J. Electrochem. Sci.*, 7(2012) 3737.
15. I. Podlubny, Fractional Differential Equations, *Academic Press*, (1999) San Diego, USA.
16. M. A. S. Aboelela, M. F. Ahmed, H. T. Dorrah, *J. Adv. Res.*, 3 (2012) 225.
17. I. Pan, S. Das. *IEEE Trans. Smart. Grid.*, 6 (2014) 36.
18. Y. Tang, M. Cui, C. Hua, L. Li and Y. Yang, *Expert. Syst. Appl.*, 39 (2012) 6887.
19. I. Pan, S. Das, *Int. J. Elec. Power.*, 43 (2012) 393.
20. H. Cao, Z. Deng, X. Li, J. Yang and Y. Qin, *Int .J. Hydrogen. Energ.*, 35 (2010) 1749.
21. Z. Deng, H. Cao, X. Li, J. Jiang and J. Yang, *J. Power Sources.*, 195 (2010) 8097.
22. D. Valério, J. S. D. Costa, *IET. Control. Theory. A.*, 152 (2005) 539.

23. Y. Q. Chen, B. M. Vinagre, *Signal Process.*, 83 (2002) 2359.
24. B. Maâmar, M. Rachid, *Isa. T.*, 53 (2014) 1620.
25. A. Oustaloup, F. Levron, B. Mathieu and F. M. Nanot, *IEEE Trans. Circuits. Syst. I, Fundam. Theory. Appl.*, 47 (2000) 25.
26. D. Y. Xue, C. N Zhao, *Control. Theory. A.*, 24 (2007) 771.
27. K. Senthilnathan, I. Annapoorani, *IET. Gener. Transm. Dis.*, 10 (2016) 2622.
28. K. Hu, L. Qi, R. Ji, J. Song and Z. Fu. *Intell. Autom. Soft. Co*.,16 (2010) 1023.
29. C. Kunusch, P. Puleston, M. Mayosky, *IEEE Trans. Energy. Conver.*, 26 (2012) 851.
30. S. Das, Functional Fractional Calculus, *Spinger-Verlag*, (2011) Berlin, Germany.
31. P. J. Torvik, R. L. Bagley, *Int. J. Appl. Mech*., 51 (1984) 725.